Nanoscale Advances

ROYAL SOCIETY OF CHEMISTRY

PAPER

View Article Online
View Journal | View Issue

Cite this: *Nanoscale Adv.*, 2026, **8**, 524

Structural morphology of nanoclay films at the air–water interface under varying ionic compositions of the subphase medium

Akash Mishra,[a] Rijul Roychowdhury,[b] Miho Tagawa[c] and Sunita Srivastava *[d]

LAPONITE®, a disc-shaped clay with uneven charge distribution, demonstrates gelation behavior that is strongly influenced by the ionic strength and pH of the suspension. These factors affect the charge on the edges and faces of the clay particles, thereby impacting electrostatic interactions and colloidal stability. In this study we investigate the adsorption behavior of the nanoclay particles on the positively charged lipid layer at the air–water interface under varying subphase ionic compositions. The Π–A compression isotherms of the nanoclay layer adsorbed on the lipid monolayer, on various subphases (water, saline, and basic), were obtained using the Langmuir method. Compression isotherms reveal that the basic subphase (pH 10) enhances nanoclay adsorption through strong electrostatic interactions between negatively charged LAPONITE® particles and the positively charged DMTAP monolayer. Films from the saline subphase (1 mM NaCl; pH $\sim$ 7) show moderate adsorption due to salt-induced charge neutralization while the water subphase (pH $\sim$ 7) exhibits minimal particle–surface interaction. The in-plane surface morphology and out-of-plane structural characteristics of nanoclay films were characterized *ex situ* by Atomic Force Microscopy (AFM) and X-Ray Reflectivity (XRR) respectively. AFM analysis reveals increasing nanoclay density with concentration across all subphases, with distinct morphological transitions influenced by subphase conditions. Films formed on pure water remain relatively uniform, while saline and basic subphases yield increasingly heterogeneous structures at higher nanoclay concentrations, with maximum heterogeneity observed in films from basic subphase. XRR unravels increased thickness and roughness in basic solution-based films, validating lateral aggregation observed in AFM micrographs. These findings highlight the role of subphase composition in modulating interfacial properties and clustering behavior in lipid–nanoclay systems.

Received 18th July 2025
Accepted 1st November 2025

DOI: 10.1039/d5na00689a

rsc.li/nanoscale-advances

Introduction

Colloidal clays, when mixed with water, form a gelatinous, liquid-like state and have emerged as a complex model system with a rich phase diagram encompassing liquid, gel, and glass phases.[1–5] Smectite clay minerals, in particular, exfoliate easily into discrete layers when dispersed in water at low concentrations; the clay nanosheets are negatively charged and $\sim$1 nm thick. LAPONITE®, a synthetic smectite clay, consists of nano-sized zwitterionic platelets with an aspect ratio of 1 : 25 and carries a positive charge on the rim and a negative charge on the face. They interlink in a colloidal suspension due to electrostatic attraction, forming a "house of cards" structure.[2,6] Higher ionic concentrations further increase cluster size, and at high concentrations, the LAPONITE® solution crystallizes.[6–8]

Most studies on LAPONITE® focus on bulk-phase gelation,[9,10] with limited research on its structural properties under 2D confinement.[1,11,12] The viscoelastic properties of LAPONITE® gels and the liquid-to-gel transition,[13] as well as interactions with various polymers and film formation of organo-clay *via* the electrospray technique,[14–16] have also been examined. While these studies primarily address gelation dynamics in the bulk phase, the gelation dynamics under 2D confinement remain largely unexplored. Recent advancements in assembly techniques, including Layer-by-Layer (LbL) and Langmuir–Blodgett (LB), have been employed to fabricate biomembrane–nanoclay thin films, with electrostatic interactions between the biomembrane and LAPONITE® playing a crucial role in monolayer formation at the interface.[17,18] The LbL method enables simple construction of multilayered films with substantial clay or organic content, although it offers limited control over molecular precision, making it more suitable for thicker, composite films. Conversely, the LB technique attains a high degree of molecular organization and layer uniformity, making

[a]*Center for Research in Nanotechnology & Science, Indian Institute of Technology Bombay, India*
[b]*Raja Ramanna Centre for Advanced Technology, Indore, Madhya Pradesh, India*
[c]*Institute of Materials and Systems for Sustainability Division of Materials Research, Nagoya University, Nagoya, Aichi, Japan*
[d]*Department of Physics, Indian Institute of Technology Bombay, Powai, Mumbai 400076, India. E-mail: sunita.srivastava@iitb.ac.in; Tel: +91 022 2576 7572*

it optimal for applications that demand precise spatial arrangement and structural regularity.

In the present work, we report the assembly of LAPONITE® (LP) particles on the surface of three different subphases: water, saline, and basic. The *in situ* interaction dynamics of the lipid–nanoclay system were characterized by using Langmuir monolayer compression isotherms, which reveal the adsorption of LAPONITE® at the interface. The *ex situ* structural analysis of films transferred from different subphases was conducted using atomic force microscopy (AFM) and X-ray reflectivity (XRR) techniques. AFM measurements validate nanoclay adsorption at the interface across all subphases, with films from the water subphase showing greater uniformity at higher LP concentrations. Films transferred from the saline subphase show larger clusters compared to those from the water subphase. However, increasing LP concentration in the basic subphase demonstrates lateral aggregation of LP particles at the interface. XRR analysis corroborates the AFM measurements, showing an increase in electron density (ED) of the organo-clay film with increasing LP concentration in the subphase.

Materials and methods

Materials

A solution containing 0.2 mg of positively charged lipid 1,2-dimyristoyl-3-trimethylammoniumpropane (DMTAP; Fig. S1) with a molecular weight of 590.4 g mol^{-1} (14 : 0 TAP, Avanti Polar) was prepared by dissolving it in 2 ml of chloroform (HPLC grade, Merck). This lipid solution was utilized for monolayer formation at the air/water interface. Sodium chloride (NaCl) and sodium hydroxide (NaOH), purchased from Merck, were used to prepare the saline and basic subphase, respectively. LAPONITE® nanoclay (*BYK Additives*; Fig. S1) was dissolved in the subphase to facilitate interaction with the lipid at the interface. The air water interface was formed using ultrapure deionized water (Millipore, resistivity = 18.2 MΩ). All glassware utilized in the experiments was thoroughly cleaned with isopropyl alcohol (IPA), acetone, and deionized water (DI water).

Subphase and LAPONITE® solution preparation

Three distinct subphases (water, saline and basic) were prepared to investigate the dynamics of DMTAP–LP films on their interface. The water subphase was prepared by directly utilizing DI water as the subphase, while the saline and basic subphases involved introducing NaCl and adjusting the pH of the subphase, respectively. In the saline subphase, NaCl was mixed into the DI water to achieve a final salt concentration of 1 mM in the subphase. The pH of DI water and the saline subphase was estimated to be similar (~7), while for the basic subphase, the pH of DI water was kept constant at 10 by adding NaOH solution to the subphase. The LAPONITE® solutions were prepared separately in each subphase by dissolving an appropriate quantity of LAPONITE® and vigorously stirring it at 1000 rpm for about one hour until a transparent solution was obtained.

DMTAP–LP film at different subphases

The DMTAP monolayer was formed on a Langmuir mini trough coated with Teflon (Biolin Scientific), equipped with symmetric hydrophilic Delrin barriers, and the surface pressure was measured using a paper Wilhelmy plate (Whatman paper) of perimeter 20.6 mm. Before monolayer formation, different subphases (~200 ml) were added to the trough, and the surface of the subphase was cleaned *via* an aspirator until a final surface pressure of ≤0.2 mN m^{-1} was reached. Following that 50 μl DMTAP solution (0.2 mg ml^{-1}) was evenly spread on the subphase.[19–21] The monolayer was then allowed to settle undisturbed for ~30 min, to ensure complete evaporation of chloroform from the surface. The surface pressure *vs.* mean molecular area (*Π–A*) isotherm was recorded through controlled compression of barriers at a speed of 5 mm min^{-1}. This recorded compression isotherm was used as a control for all DMTAP–LP systems. For preparing DMTAP–LP films, a small volume of stock LAPONITE® solution of concentration 11 mg ml^{-1} (*e.g.*, 15 mL for the 0.05 wt% LP) was first prepared separately and thoroughly mixed until a transparent and homogeneous solution was obtained. This pre-mixed LP solution was then gently introduced into the subphase of the Langmuir trough from one side of the barrier, while an equivalent volume of the subphase (10 mL) was simultaneously removed from the opposite side of another barrier to maintain a constant total volume (~200 mL) in the trough. Different volumes of the LP solution were then added in the subphase, resulting in final nanoclay concentrations of 0.05 wt%, 0.16 wt%, 0.38 wt% and 0.5 wt% in the subphase. To ensure uniform diffusion and interaction of the LAPONITE® particles with the pre-formed DMTAP monolayer across the entire interface, the system was allowed to equilibrate undisturbed for approximately 6 hours. This prolonged interaction time allowed for sufficient mixing and adsorption of nanoclay particles onto the monolayer. We arrived at this specific equilibration time through a series of preliminary experiments (Fig. S2). Our criterion was that, after introducing particles to the subphase, the lift-off area showed no further notable change with time.

The *ex situ* structural morphology of lipid–nanoclay composite films was investigated by transferring them from the interface using the Langmuir–Schaefer (LS) technique.[22] The films were transferred at a surface pressure of 5 mN m^{-1} onto piranha-cleaned silicon substrates held horizontally by an automated dipper, with the polished side in contact with the water surface (Fig. S3). The transfer speed was maintained at 2 mm min^{-1} for both upward and downward movements. Atomic Force Microscopy (AFM) in tapping mode at room temperature was used to characterize the surface morphology of the films.[23] For all AFM measurements, the tip resonance frequency was set at 70 kHz, with a scan speed of 1 Hz and a scan size of 256 × 256 pixels. Different areas of the film were scanned within regions of 5 μm × 5 μm and 1 μm × 1 μm. The AFM images were processed and analyzed using Gwyddion software.[24] Additionally, the out-of-plane XRR measurement of the DMTAP–LP complex was conducted using a synchrotron source at the Grazing Incidence X-ray Scattering (GIXS) beamline, BL-13, Indus-2, RRCAT Indore, with a photon energy of 10 keV ($\lambda \approx 1.23$ Å). Data were

recorded under specular conditions, keeping the incident and reflection angles constant (θ), ensuring that the scattering occurred in the same plane to provide the vertical wave vector q_z, whose value is given as

$$q_z = \frac{4\pi}{\lambda}\sin\theta \quad (1)$$

The recorded data consist of various defects due to the beam profile and geometric factor of the instrument, known as the spill-over effect, which needs to be corrected.[25,26] Thus the recorded data was first normalized to remove the defects, and then compared with Fresnel reflectivity for a flat surface, $R(\theta)$ given as

$$R(\theta) = \frac{\left|\theta - \sqrt{\theta^2 - 2\delta + 2i\beta}\right|^2}{\left|\theta + \sqrt{\theta^2 - 2\delta + 2i\beta}\right|^2} \quad (2)$$

where δ and β are the dispersion and absorption constant of the film, respectively. The calculated normal wave vector q_z at the critical angle θ_C for bare silicon substrate from the normalized reflectivity profile is 0.3 $Å^{-1}$ (Fig. S4). The normalized reflectivity profiles were compared with theoretical Fresnel reflectivity for a flat surface and analyzed using Parratt's formalism, where the film is assumed to be a stack of multiple layers with sharp interfaces (inset of Fig. S9(b)).[26,27] The profiles were modelled for multiple interfaces using the Moto fit package in IgorPro software.[28]

Results and discussion

Structural analysis of lipid–nanoclay films

***In situ* compression isotherm for the DMTAP–LP film.** The Langmuir–Bodgett (LB) technique is utilized to measure the Langmuir monolayer compression isotherm of the lipid–nanoclay system at the interface as it is widely recognized as one of the best methods for controlled measurement at the interfaces.[29,30] Fig. 1 shows the typical compression isotherm and static elastic modulus (E) of the DMTAP monolayer and DMTAP–LP complex monolayer at the interface. The static elastic modulus (E) is calculated using;

$$E = -A\frac{d\Pi}{dA} \quad (3)$$

where Π and A are the surface pressure and mean molecular area (MMA) of the film during compression, respectively.

The compression isotherms reveal the transition of monolayers across distinct two-dimensional phases as shown in Fig. 1(a). The gaseous (G) phase represents the region where molecules are sufficiently separated, resulting in negligible interaction with neighboring molecules. Upon compression, we measure an increase in surface pressure due to enhanced intermolecular interactions. The mean molecular area (MMA) at which surface pressure begins to increase is termed as the lift-off area (A_0), which defines the transition of the film from the gaseous phase to the liquid-expanded (LE) phase, marking the onset of intermolecular interaction within the film. On further compression, both monolayers transition through liquid-expanded (LE) and liquid-condensed (LC) phases before the monolayers collapsed (C). The measured A_0 for the pure lipid film is approximately 100 $Å^2$, aligning with prior studies on DMTAP monolayers.[12] For the DMTAP–LP monolayer, A_0 shifts to ~130 $Å^2$, due to nanoclay adsorption at the interface. The static elastic modulus (Fig. 1(b)) using eqn (3) indicates a higher value of $|E|_{max}$ for the DMTAP and DMTAP–LP films with estimates of 90 mN m^{-1} and 100 mN m^{-1} respectively, showing the higher mechanical stability of the lipid–nanoclay film than the lipid film.[12,31] The higher $|E|_{max}$ observed for the DMTAP–LP monolayer arises from the increased rigidity imparted by nanoclay adsorption at the interface. LAPONITE® platelets, with their disc-like shape and anisotropic charge distribution (negatively charged basal surfaces and positively charged rims), adsorb *via* electrostatic interactions onto the cationic DMTAP monolayer, reinforcing lateral cohesion within the film. This interaction reduces molecular mobility, thereby increasing the resistance to compression, which manifests as higher elastic modulus values for DMTAP–LP films compared to the pure DMTAP monolayer. The transition between different phases, as observed in the isotherm (Fig. 1(a)), is reflected in the changing slopes of the *E vs.* MMA curve (Fig. 1(b)). Furthermore, the estimates of E_{max} were found to increase with LP concentration indicating enhanced adsorption of the LP particles at the interface (Fig. S5).

Fig. 2(a–c) shows the Π–A isotherms of DMTAP–LP films with varying LP concentrations in water, saline, and basic subphases, respectively. The lift-off area (A_0) increases with increasing LP concentrations for all subphases, confirming the enhanced adsorption of LP particles onto the DMTAP monolayer. For the water subphase, the A_0 values at 0.05%, 0.16%, and 0.38% LP concentrations are ~130 $Å^2$, 158 $Å^2$, and 167 $Å^2$, respectively. On the saline and basic subphases, the corresponding A_0 values are ~155 $Å^2$, 166 $Å^2$, and 176 $Å^2$ for the saline subphase, and ~136 $Å^2$, 182 $Å^2$, and 198 $Å^2$ for the basic subphase, respectively. For the pure DMTAP monolayer, A_0 is ~100 $Å^2$, as mentioned above. The maximum change in the lift-off area, ΔA_0, is calculated by taking the difference between the A_0 value of the monolayer with the maximum LP concentration and that of the pure DMTAP monolayer (Fig. 2(d)). The ΔA_0 estimates for water and saline are ~67 $Å^2$

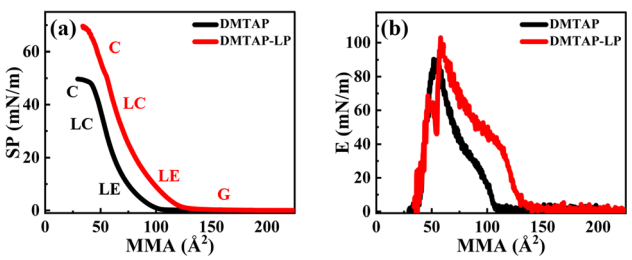

Fig. 1 (a) Π–A isotherm of a pure DMTAP film and DMTAP–LP monolayer. Different 2D phases from gaseous (G) to liquid-condensed (LC) are observed before the monolayer collapses (C). (b) The static modulus (E) isotherm of monolayers calculated from the compression isotherm. Higher $|E|$ for the DMTAP–LP monolayer reveals increased rigidity of the film.

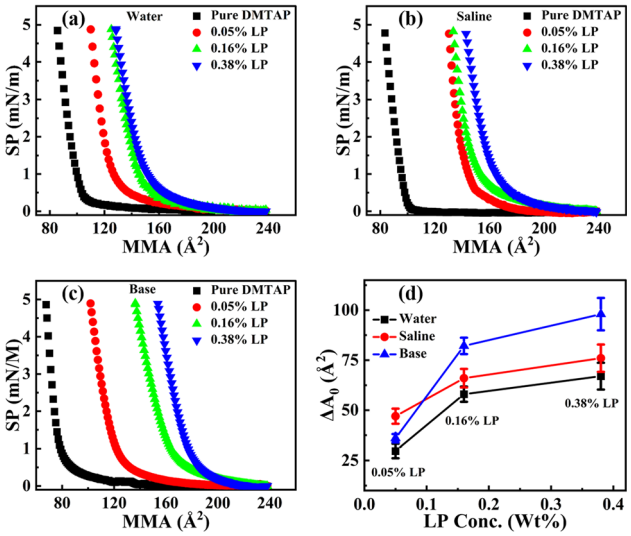

Fig. 2 (a–c) The compression profile of a DMTAP–LP film with varying LAPONITE® wt% on the water, saline and basic subphases, respectively. (d) The increment in lift-off area (ΔA_0) with increasing nanoclay concentration in water, saline and basic subphases. Maximum increment in lift-off area (A_0) is observed in the basic subphase indicating the highest adsorption of LP platelets on the interface.

and ~75 Å^2 respectively, with a maximum measured shift of ~100 Å^2 for the basic subphase. The adsorption of LP particles at the interface is facilitated by the electrostatic attraction between the negatively charged basal surface of the particle and the positively charged lipid layer. The positively charged edges of the LP particles hinder their adsorption at the interface, but promote interparticle interaction in the subphase, which depends on particle density. It has been found in the literature that at high concentration, LP particles form clusters of the house-of-card structure due to attractive interaction between the basal surface and edges of neighboring particles.[2,6,32] These interparticle interactions are tunable through concentration,[33,34] salinity[35,36] and pH[37,38] of the subphase as has been reported in the literature for bulk solutions.

The interplay of particle–particle interactions in the subphase and particle–surface attraction will control the surface adsorption of LP particles. For the water subphase the interparticle attraction due to the negatively charged basal surface and positively charged edges is maximum, as compared to saline and basic subphases. The marginal increase in the adsorption of LP particles for the saline subphase compared to that of water can be attributed to the screened interparticle attraction which shall promote better surface adsorption. In the basic subphase (pH 10), LP particles are fully deprotonated due to the abundance of OH^- ions, increasing the negative charge density of the LP particles, which strengthens electrostatic attraction with the positively charged interface, thereby enhancing nanoclay adsorption. The particles in the subphase are stabilized through repulsive interparticle interaction.[39] This interaction strength promoting the colloidal stability in the subphase is maximum for the basic subphase, followed by saline and water subphases. We observe that, at a fixed particle concentration, a reduction in interparticle interaction strength—driven by subphase composition—leads to an increase in surface adsorption.

Surface morphology analysis of the DMTAP–LP film. The AFM micrographs for surface morphology study of the DMTAP–LP films transferred from water, saline, and basic subphases at varying LP concentrations (0.05 wt%, 0.38 wt%, and 0.5 wt%) are shown in Fig. 3. It is evident from the AFM data that for all subphase conditions, the particle adsorption at the interface increases with increasing LP concentration. Individual LAPONITE® nanoclay particles are disc-shaped, with diameters of ~25–30 nm and a thickness of ~1 nm. The AFM data reveal that the clay particles form an aggregated cluster at the interface. The size of the cluster, measured from high magnification images of the DMTAP–LP film transferred from the water subphase (Fig. S7), is ~100 nm. We find that this size is larger than the size of the individual particle, probably because of strong electrostatic interparticle attraction between nanoclays. Our estimates suggest that the cluster sizes are ~3–4 particles in the water subphase. Furthermore, we observe that the DMTAP–LP films (Fig. 3(a–c)) exhibit a disordered arrangement of nanoclay clusters. To quantify the surface coverage of nanoclay films transferred from different subphases at varying nanoclay concentrations, we selected the threshold height of ~3 nm (Fig. S8) at which surface density and lateral cluster size are estimated, unless mentioned otherwise. As the concentration of LP increases from 0.05% to 0.38%, the surface density estimates of the LP cluster increase from ~13% to ~16%, leading to a gradual transition toward a more compact and homogeneous film. The estimates of the cluster size and the surface coverages are obtained using the ImageJ analysis software.[40]

Similar to the water subphase, films transferred from the saline subphase (Fig. 3(d–f)) show formation of LP clusters at the interface. On increasing LP concentration in the subphase, from 0.05% to 0.38%, the estimated density of the LP cluster increases from ~10% to ~22%. At 0.5% LP, the high density of the surface films makes it impossible to get an error-free estimate of the cluster size and surface coverage. At low concentrations, both the systems exhibit nearly similar coverage, with considerably large nanoclay cluster density at enhanced LP concentration in the saline subphase compared to water. This is consistent with the results from *in situ* isotherms as discussed above, where a higher shift in lift-off area has been measured for saline compared to water. Notably, we found that the LP films from the saline subphase are relatively more heterogeneous compared to water. The heterogeneity in the surface film increases with increasing concentration of particles in the subphase (Fig. 3(d–f)). Unlike water and saline, monolayers transferred from the basic subphase, pH 10 (Fig. 3(g–i)), exhibit smaller LP clusters (Fig. S6) and a homogeneous film at low LP concentrations. However, with an increase in LP concentration we observe the formation of heterogeneous films. The LP particles in the basic solution (pH 10) are known to exhibit uniform negative charge on both the basal surface and edges of the disc particles.[2,38] Under these conditions, the particles in the subphase are stabilized by repulsive interactions. However, compared to water and saline subphases, enhanced electrostatic attraction with the lipid surface is expected. This accounts for the smaller cluster size and the higher particle surface density. The adsorption of particles at

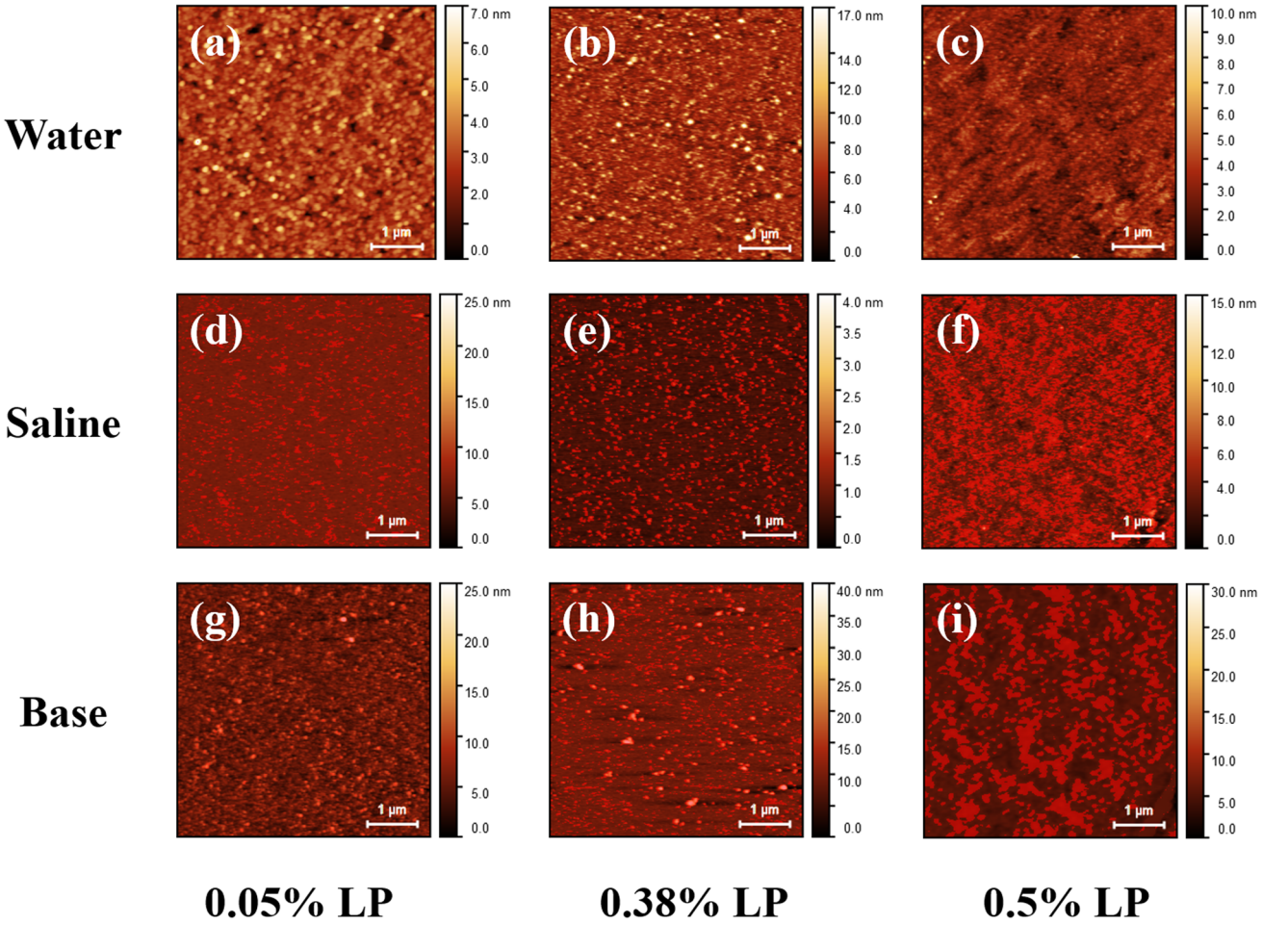

Fig. 3 Surface morphology of films transferred from different subphases at varying LP concentrations. (a–c) Films transferred from the water subphase; (d–f) films transferred from the saline subphase; and (g–i) films transferred from the basic subphase, respectively (scan size: 5 μm × 5 μm). High magnification images of corresponding films are shown in the SI (Fig. S6).

the interface increases with concentration, resulting in density-driven aggregation and the formation of a heterogeneous film at high concentrations. Interestingly, although heterogeneous films are observed in both saline and basic subphase systems, the mechanisms underlying their formation differ. In the saline system, cluster formation is primarily driven by enhanced inter-particle interactions between the oppositely charged basal surfaces and edges, leading to cluster growth. In contrast, in the basic system, aggregation occurs due to an increase in particle density, driven by enhanced adsorption at the surface as a result of stronger surface and particle interactions. Thus we see heterogeneous films for saline at all concentration (Fig. 3(d–f)) whereas for a basic subphase this phenomenon is observed at higher concentration (Fig. 3(i)). Our results provide insights into the adsorption mechanism of nanoclay particles that are driven by dominant particle–surface and particle–particle interactions depending on the ionic composition of the subphase.

Out-of-plane XRR analysis of DMTAP–LP films. The normalized XRR data for DMTAP–LP films at varying concentrations of LP (0.05% LP, 0.38% LP and 0.5% LP) transferred from water, saline and basic subphases are shown in Fig. 4(a–c), respectively. The solid lines are fit to the data, using the Parratt algorithm[20,22,26,27] to extract information regarding film thickness, density and composition. Analysis of XRR data provides an electron density profile (EDP), which represents the in-plane average electron density (e) as a function of the out-of-plane distance/thickness of the film (Z). In this analysis, the box model used to fit the data consists of several layers, representing silicon, SiO_2, lipid tail (L_T) and a mixture of lipid head + nanoclay layer (LP + L_H) respectively (inset: Fig. 4(d–f)). The parameters obtained (Table ST1) after fitting XRR data of a bare silicon substrate (Fig. S4) were subsequently used to fit the different layers of the DMTAP–nanoclay film.[41–44]

The electron density profiles (EDPs) extracted from fitting the XRR data for the corresponding DMTAP–LP films are displayed in Fig. 4(d–f). The thickness, electron density (ED), and roughness of the lipid–nanoclay films obtained from the fit to the XRR data are shown in Table ST3. It can be seen that the thickness estimate of the LP + L_H layer varies in the range of 31–42 Å for all the systems, validating the thickness estimate of the nanoclay film from the AFM micrograph (Fig. S8). Given that the size of the lipid head group is approximately 6–8 Å, the thickness of the LP films is estimated to be in the range of 23–36 Å, indicating that LP particles interact with the lipid *via* their negatively charged basal surfaces.

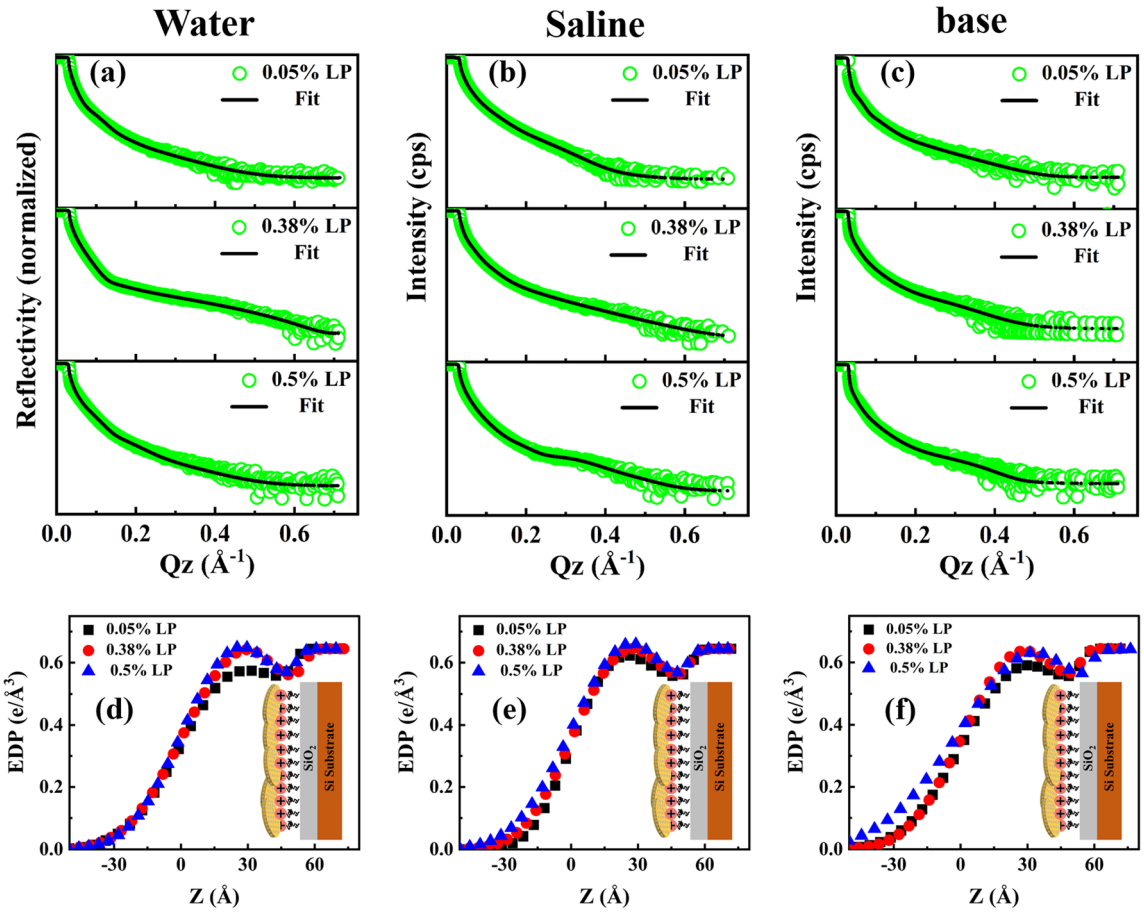

Fig. 4 (a–c) The reflectivity profile of the DMTAP–LP films transferred from different subphases (water, saline and basic respectively) with varying LP concentrations. (d–f) The extracted electron density profile (EDP) from the fitting of reflectivity data of the corresponding films using Parrat's algorithm. The inset of the EDP profiles shows the model used for fitting the data.

Furthermore, thickness estimates greater than 1 nm (the thickness of one LP particle) suggest the formation of a multilayer structure with 2–3 particle layers at the interface. The composite layer thickness was found to be weakly dependent on concentration across all systems, indicating that the out-of-plane morphology is not significantly affected by the increase in in-plane density observed in the isotherms and AFM data. The film roughness marginally depends on particle composition, however it exhibits the maximum value for the basic subphase. This trend is consistent across different subphase systems and aligns with AFM observations, which show that surface heterogeneity and film roughness increase for films formed on water, saline, and basic subphases (Table ST3).

The surface density estimate of the composite layers derived by integrating the area under the curve of the EDP profile is shown in Fig. 5. The electron density of the bare silicon substrate was used as a baseline control, allowing us to isolate and quantify the contribution from the interfacial DMTAP–LP film. This integrated value represents the total interfacial film density resulting from particle adsorption. It can be seen that the surface density consistently increases with particle concentration for all the systems. At 0.5 wt% LP on pure water, the slight decrease in surface density likely arises from increased interfacial roughness and

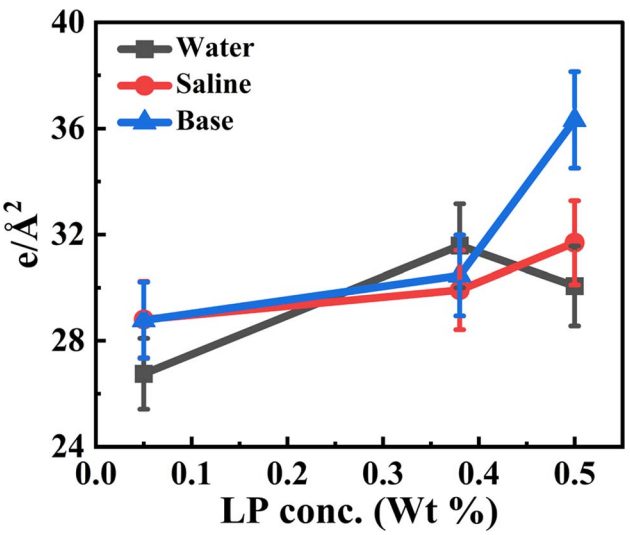

Fig. 5 Electron density per unit area for DMTAP–LP films transferred from different subphases at various LP concentrations. Electron density is the highest in the nanoclay film transferred from the basic subphase at 0.5% LP indicating enhanced LP adsorption at the interface.

heterogeneous coverage, which can reduce the apparent electron density in XRR analysis. These observations are consistent with AFM and isotherm data, reflecting similar trends in in-plane and out-of-plane structural features.

Conclusion

This study illustrates how the ionic composition of the subphases (water, saline, and basic) influences the adsorption, clustering, and structural properties of lipid–nanoclay films. The basic (pH 10) subphase facilitates negative charge on both the basal and edge surface of the nanoclay particle, thus enhancing the overall negative surface charge density of the particle. As a result, maximum nanoclay adsorption was measured for the basic subphase because of strong electrostatic interactions between negatively charged LAPONITE® particles and the positively charged DMTAP lipid film. The particles in the basic subphase are stabilized by repulsive interactions. The interfacial particle adsorption for the saline and water subphase (both having pH $\sim$ 7) is similar, with marginally higher estimates for the saline subphase. These results suggest that a stable colloidal dispersion facilitates the adsorption of the particles on charged surfaces and the choice of dispersion for adsorption of nanoclay particles in increasing order of affinity are water, saline and basic.

AFM analysis showed disordered LAPONITE® clusters in films from the water subphase at the lowest LP concentration, which densified into a homogeneous film with increasing particle concentration. Saline subphases resulted in heterogeneous film formation at low concentrations, with increasing heterogeneity at higher concentrations. Basic subphases, on the other hand, exhibited homogeneous film formation at low concentrations, transitioning to heterogeneous films at higher concentrations. In the case of films from basic subphases, heterogeneity appears due to an increase in interfacial density of the particles, whereas in the case of a saline system, the heterogeneous network (at low concentration) occurs because of screened interparticle repulsion in the presence of a saline environment. The out-of-plane XRR analysis corroborates the AFM findings, with the lowest electron density (ED) observed in the nanoclay layer on the water subphase. Basic and saline subphases show nearly similar ED values but higher estimates of thickness and roughness, further validating heterogeneity in the interfacial films. Overall, this study underscores the critical role of subphase modification in determining the interfacial properties and structural morphology of lipid–nanoclay films. These findings provide valuable insights into the adsorption behavior of charged complex colloids on charged surfaces under different ionic conditions.

Author contributions

Akash Mishra: data curation, formal analysis, investigation, methodology, software, visualization, writing – original draft preparation. Rijul Roychowdhury: data curation, resources. Miho Tagawa: writing – review and editing. Sunita Srivastava: conceptualization, funding acquisition, supervision, resources, project administration, validation, methodology, writing – review & editing.

Conflicts of interest

There are no conflicts to declare.

Data availability

All data generated or analyzed during this study are included in the main article and its supplementary information (SI). No additional datasets were generated or analyzed during the current study. Supplementary Information is available. See DOI: https://doi.org/10.1039/d5na00689a.

Acknowledgements

Akash Mishra acknowledges financial support from IRCC IIT Bombay. This work was partially supported by DST/JSPS/P-389/2024(G) and the joint usage/research program of the Institute of Materials and Systems for Sustainability (IMaSS), Nagoya University. SS acknowledges the financial support from CRS-DAE, India. The authors are thankful to Saha Institute of Nuclear Physics (SINP), Kolkata, for facilitating the XRR measurements at the GIXS beamline (BL-13), INDUS-2, RRCAT, Indore, India, which provide good insight for further measurements. The authors also acknowledge the Centre of Excellence in Nanoelectronics (CEN), IIT Bombay, India for facilitating the AFM measurements.

References

1 B. Ruzicka and E. Zaccarelli, A fresh look at the Laponite phase diagram, *Soft Matter*, 2011, **7**, 1268–1286.
2 H. Z. Cummins, Liquid, glass, gel: The phases of colloidal Laponite, *J. Non-Cryst. Solids*, 2007, **353**, 3891–3905.
3 E. Zaccarelli, Colloidal gels: Equilibrium and non-equilibrium routes, *J. Phys.: Condens. Matter*, 2007, **19**, 323101.
4 M. Veiskarami, M. N. Sarvi and A. R. Mokhtari, Influence of the purity of montmorillonite on its surface modification with an alkyl-ammonium salt, *Appl. Clay Sci.*, 2016, **120**, 111–120.
5 F. Sciortino and P. Tartaglia, Glassy colloidal systems, *Adv. Mater. Phys.*, 2005, **54**, 471–524.
6 K. Suman and Y. M. Joshi, Microstructure and soft glassy dynamics of an aqueous laponite dispersion, *Langmuir*, 2018, **34**, 13079–13103.
7 T. Nicolai and S. Cocard, Light scattering study of the dispersion of laponite, *Langmuir*, 2000, **16**, 8189–8193.
8 S. L. Tawari, D. L. Koch and C. Cohen, Electrical double-layer effects on the Brownian diffusivity and aggregation rate of Laponite clay particles, *J. Colloid Interface Sci.*, 2001, **240**, 54–66.
9 S. Srivastava, S. Kishore, S. Narayanan, A. R. Sandy and S. R. Bhatia, Multiple Dynamic Regimes in Colloid-Polymer Dispersions: New Insight Using X-Ray Photon Correlation Spectroscopy, *J. Polym. Sci., Part B: Polym. Phys.*, 2016, **54**, 752–760.

10 S. Kishore, S. Srivastava and S. R. Bhatia, Microstructure of colloid-polymer mixtures containing charged colloidal disks and weakly-adsorbing polymers, *Polymer*, 2016, **105**, 461–471.
11 A. Mourchid and P. Levitz, Long-term gelation of laponite aqueous dispersions, *Phys. Rev. E*, 1998, **57**, R4887.
12 C. Kumar and S. Srivastava, Structural and Dynamical Studies of a Lipid–Nanoclay Composite Layer at the Air–Water Interface, *Langmuir*, 2022, **38**, 10400–10411.
13 A. Mourchid, E. Lecolier, H. Van Damme and P. Levitz, On viscoelastic, birefringent, and swelling properties of laponite clay suspensions: Revisited phase diagram, *Langmuir*, 1998, **14**, 4718–4723.
14 A. S. Negi, C. G. Redmon, S. Ramakrishnan and C. O. Osuji, Viscoelasticity of a colloidal gel during dynamical arrest: Evolution through the critical gel and comparison with a soft colloidal glass, *J. Rheol.*, 2014, **58**, 1557–1579.
15 C. T. Johnston, Probing the nanoscale architecture of clay minerals, *Clay Miner.*, 2010, **45**, 245–279.
16 V. Can and O. Okay, Shake gels based on Laponite–PEO mixtures: effect of polymer molecular weight, *Des. Monomers Polym.*, 2005, **8**, 453–462.
17 S. Miao, F. Bergaya and R. Schoonheydt, Ultrathin films of clay–protein composites, *Philos. Mag.*, 2010, **90**, 2529–2541.
18 R. H. Ras, Y. Umemura, C. T. Johnston, A. Yamagishi and R. A. Schoonheydt, Ultrathin hybrid films of clay minerals, *Phys. Chem. Chem. Phys.*, 2007, **9**, 918–932.
19 S. Srivastava, D. Nykypanchuk, M. Fukuto, J. D. Halverson, A. V. Tkachenko, K. G. Yager and O. Gang, Two-Dimensional DNA-Programmable Assembly of Nanoparticles at Liquid Interfaces, *J. Am. Chem. Soc.*, 2014, **136**, 8323–8332.
20 S. Srivastava, D. Nykypanchuk, M. Fukuto and O. Gang, Tunable Nanoparticle Arrays at Charged Interfaces, *ACS Nano*, 2014, **8**, 9857–9866.
21 S. Srivastava, M. Fukuto and O. Gang, Liquid interfaces with pH-switchable nanoparticle arrays, *Soft Matter*, 2018, **14**, 3929–3934.
22 S. Srivastava, J. K. Basu, M. Sprung and J. Wang, Morphological transitions in polymer monolayers under compression, *J. Chem. Phys.*, 2009, **130**, 174718.
23 S. Srivastava and J. K. Basu, Buckling in polymer monolayers: Molecular-weight dependence, *Phys. Rev. E*, 2009, **79**, 041603.
24 D. Nečas and P. Klapetek, Gwyddion: an open-source software for SPM data analysis, *Open Phys.*, 2012, **10**, 181–188.
25 A. Gibaud, G. Vignaud and S. Sinha, The correction of geometrical factors in the analysis of X-ray reflectivity, *Acta Crystallogr., Sect. A:Found. Crystallogr.*, 1993, **49**, 642–648.
26 A. Das, S. D. Singh, R. Choudhari, S. Rai and T. Ganguli, Data-reduction procedure for correction of geometric factors in the analysis of specular X-ray reflectivity of small samples, *J. Appl. Crystallogr.*, 2018, **51**, 1295–1303.
27 L. G. Parratt, Surface studies of solids by total reflection of X-rays, *Phys. Rev.*, 1954, **95**, 359.
28 A. Nelson, Co-refinement of multiple-contrast neutron/X-ray reflectivity data using MOTOFIT, *J. Appl. Crystallogr.*, 2006, **39**, 273–276.
29 G. Roberts, *Langmuir-Blodgett Films*, Springer Science & Business Media, 2013.
30 O. N. Oliveira Jr, L. Caseli and K. Ariga, The past and the future of Langmuir and Langmuir–Blodgett films, *Chem. Rev.*, 2022, **122**, 6459–6513.
31 E. Guzmán, L. Liggieri, E. Santini, M. Ferrari and F. Ravera, Mixed DPPC–cholesterol Langmuir monolayers in presence of hydrophilic silica nanoparticles, *Colloids Surf., B*, 2013, **105**, 284–293.
32 P. H. Michels-Brito, A. Malfatti-Gasperini, L. Mayr, X. Puentes-Martinez, R. P. Tenório, D. R. Wagner, K. D. Knudsen, K. Araki, R. G. Oliveira, J. Breu, *et al.*, Unmodified clay nanosheets at the air–water interface, *Langmuir*, 2020, **37**, 160–170.
33 P. Mongondry, J. F. Tassin and T. Nicolai, Revised state diagram of Laponite dispersions, *J. Colloid Interface Sci.*, 2005, **283**, 397–405.
34 P.-I. Au, S. Hassan, J. Liu and Y.-K. Leong, Behaviour of LAPONITE® gels: rheology, ageing, pH effect and phase state in the presence of dispersant, *Chem. Eng. Res. Des.*, 2015, **101**, 65–73.
35 A. Y. Huang and J. C. Berg, High-salt stabilization of Laponite clay particles, *J. Colloid Interface Sci.*, 2006, **296**, 159–164.
36 B. Ruzicka, L. Zulian and G. Ruocco, Ageing dynamics in Laponite dispersions at various salt concentrations, *Philos. Mag.*, 2007, **87**, 449–458.
37 A. Pek-Ing and L. Yee-Kwong, Surface chemistry and rheology of Laponite dispersions—Zeta potential, yield stress, ageing, fractal dimension and pyrophosphate, *Appl. Clay Sci.*, 2015, **107**, 36–45.
38 S. Jatav and Y. M. Joshi, Chemical stability of Laponite in aqueous media, *Appl. Clay Sci.*, 2014, **97**, 72–77.
39 T. Tadros, Interparticle interactions in concentrated suspensions and their bulk (Rheological) properties, *Adv. Colloid Interface Sci.*, 2011, **168**, 263–277.
40 M. D. Abràmoff, P. J. Magalhães and S. J. Ram, Image processing with ImageJ, *Biophotonics Int.*, 2004, **11**, 36–42.
41 R. J. Sarmah and S. Kundu, Stable layers of pure myelin basic protein (MBP): Structure, morphology and hysteresis behaviors, *Colloids Surf., A*, 2023, **662**, 130973.
42 H.-C. Lee, T.-W. Lee, T.-H. Kim and O. O. Park, Fabrication and characterization of polymer/nanoclay hybrid ultrathin multilayer film by spin self-assembly method, *Thin Solid Films*, 2004, **458**, 9–14.
43 K. Glinel, A. Laschewsky and A. M. Jonas, Ordered polyelectrolyte "multilayers". 3. Complexing clay platelets with polycations of varying structure, *Macromolecules*, 2001, **34**, 5267–5274.
44 J.-y. Hasegawa, T. Kawatsu, K. Toyota and K. Matsuda, Chemical-intuition based LMO transformation simplifies excited-state wave functions of peptides, *Chem. Phys. Lett.*, 2011, **508**, 171–176.